On the Seasonal Cycle of the Statistical Properties of Sea Surface Temperature

Jordi Isern-Fontanet, Xavier Capet, Antonio Turiel, Estrella Olmedo, Christina González-haro

Geophysical Research Letters

RESEARCH LETTER
10.1029/2022GL098038

On the Seasonal Cycle of the Statistical Properties of Sea Surface Temperature

J. Isern-Fontanet[1,2], X. Capet[3], A. Turiel[1,2], E. Olmedo[1,2], and C. González-Haro[1,2]

[1]Institut de Ciències del Mar (CSIC), Barcelona, EU, [2]Barcelona Expert Centre in Remote Sensing, Barcelona, EU, [3]LOCEAN, Paris, EU

Key Points:

- The intensity of Sea Surface Temperature (SST) fronts is quantified using singularity exponents, which measure the continuity of the field
- Anomalous scaling of SST structure functions is correlated to the the intensity of the strongest fronts
- The variability of the strongest fronts depends on the seasonal variability of the coastal upwelling in the area of study

Correspondence to:
J. Isern-Fontanet,
jisern@icm.csic.es

Citation:
Isern-Fontanet, J., Capet, X., Turiel, A., Olmedo, E., & González-Haro, C. (2022). On the seasonal cycle of the statistical properties of Sea Surface Temperature. *Geophysical Research Letters*, *49*, e2022GL098038. https://doi.org/10.1029/2022GL098038

Received 25 JAN 2022
Accepted 7 APR 2022

Author Contributions:
Conceptualization: J. Isern-Fontanet
Data curation: J. Isern-Fontanet, X. Capet
Formal analysis: J. Isern-Fontanet
Funding acquisition: J. Isern-Fontanet
Investigation: J. Isern-Fontanet, X. Capet, A. Turiel, E. Olmedo, C. González-Haro
Methodology: J. Isern-Fontanet, X. Capet, A. Turiel, E. Olmedo
Project Administration: J. Isern-Fontanet
Resources: J. Isern-Fontanet
Software: J. Isern-Fontanet, A. Turiel
Supervision: J. Isern-Fontanet
Validation: X. Capet
Visualization: J. Isern-Fontanet
Writing – original draft: J. Isern-Fontanet

Abstract The contribution of ocean fronts to the properties and temporal evolution of Sea Surface Temperature (SST) structure functions have been investigated using a numerical model of the California Current system. First, the intensity of fronts have been quantified by using singularity exponents. Then, leaning on the multifractal theory of turbulence, we show that the departure of the scaling of the structure functions from a straight line, known as anomalous scaling, depends on the intensity of the strongest fronts. These fronts, at their turn, are closely related to the seasonal change of intensity of the coastal upwelling characteristics of this area. Our study points to the need to correctly reproduce the intensity of the strongest fronts and, consequently, properly model processes such as coastal upwelling in order to reproduce SST statistics in ocean models.

Plain Language Summary Forecasting the evolution of the Earth's climate requires to predict the evolution of the statistical characteristics of essential climate variables such as the Sea Surface Temperature. In this study, it has been found that some of such statistical properties depend on the intensity of the strongest fronts in the ocean. This implies that those ocean, or climate, models that fail to correctly predict their intensity will not be able to correctly reproduce the statistical characteristics of key variables such as temperature. The area analyzed in this study is the California Current system, where the strongest fronts are modulated by the seasonal evolution of the upwelling. Therefore, our results imply that such a system has to be correctly modeled, or parametrized, in order to properly reproduce the statistics of ocean temperatures.

1. Introduction

Sea Surface Temperature (SST) is a fundamental variable of the Earth climate system due to its role in regulating climate and weather (Deser et al., 2010) and its dynamical connection to ocean currents (Isern-Fontanet et al., 2014). Moreover, the availability of a long time series of global high resolution satellite measurements of SST (Merchant et al., 2019) makes it well suited for addressing a wide range of problems such as monitoring Climate Change (Gulev et al., 2021); retrieving ocean currents (Isern-Fontanet et al., 2017); or calibrating and validating ocean and climate models (Skákala et al., 2019). It is, therefore, of major importance to understand how ocean processes contribute to SST statistics to exploit such a wealth of data and get insight into the functioning of the ocean and climate.

A prominent feature of SST is the presence of fronts, which are known to be sinks of energy (D'Asaro et al., 2011; Isern-Fontanet & Turiel, 2021) and significantly contribute to the vertical transport of nutrients and, thus, to primary production (Mahadevan, 2016). The variability of the characteristics of fronts, such as the density of fronts or their intensity, are expected to be mirrored by the variability of some SST statistics. A popular approach is based on the spectral slope of SST because it can be connected to theories of turbulence. Nevertheless, they provide an incomplete framework, if only because different theories may predict the same slope (Callies & Ferrari, 2013) and the underlying turbulence regime may not change in spite of the seasonal changes in the properties of fronts.

The structure functions of a turbulent variable, that is, the moments of the differences between two points, are also at the core of theories of turbulence (Pope, 2000) and extend the information provided by spectral slopes (Sukhatme et al., 2020; Yu et al., 2017). Moreover, the anomalous scaling of the power laws deduced from the structure functions, that is, its deviation from a straight line, can be related to the geometry of gradients making use of the multifractal framework (Isern-Fontanet & Turiel, 2021). The relevance of this approach has already been demonstrated in the oceanic context (Isern-Fontanet et al., 2007), and it has been used to develop metrics for

Writing – review & editing: J. Isern-Fontanet, X. Capet, A. Turiel, E. Olmedo, C. González-Haro

model validation (Ivanov et al., 2009; Skákala et al., 2016), although it has not been yet exploited to investigate the contribution of fronts to SST statistics.

Here, we introduce a metric to measure the intensity of SST fronts in numerical simulations of the California Current System (Capet et al., 2008), which is dominated by cross-shore gradients generated by coastal upwelling (Chenillat et al., 2018). This metric is then connected to the scaling of the structure functions using the multifractal framework (Frisch, 1995) and used to investigate how the temporal variability of front intensity contribute to the variability of anomalous scaling and spectral slopes. The paper is organized as follows: Section 2 puts the multifractal theory of turbulence in the context of oceanography; Section 3 describes the numerical simulations and the algorithms used for this study; Sections 4 and 5 describe results and discuss them, respectively; and Section 6 list the conclusions.

2. Theoretical Framework

Coarse-grained SST gradients are built by filtering the module of the thermal gradient as

$$\overline{|\nabla T|}_{\ell}(\vec{x}) \equiv \int_{\mathbf{R}^d} \ell^{-d} G\left(\ell^{-1}\vec{x}\right) |\nabla T|\left(\vec{x}+\vec{x}'\right) d\vec{x}', \tag{1}$$

where $d = 2$ is the geometrical dimension; ℓ is the scale of the filter; $G\left(\vec{x}\right)$ is a normalized positive function that decays fast to zero as $|\vec{x}| \to \infty$; $T\left(\vec{x}\right)$ is the SST; and $\nabla = (\partial_x, \partial_y)$. These SST gradients are known to possess a range of scaling exponents $h\left(\vec{x}\right)$ that verify

$$\overline{|\nabla T|}_{\ell}(\vec{x}) \sim \left(\frac{\ell}{\ell_0}\right)^{h(\vec{x})} \tag{2}$$

as $\ell/\ell_0 \to 0$, where ℓ_0 is the integral scale of the flow (Isern-Fontanet et al., 2007). The scaling exponents $h\left(\vec{x}\right)$, known as singularity or Hölder exponents, quantify the degree of continuity of SST. Indeed, if $h\left(\vec{x}\right) \in (n, n+1)$ with n being a positive integer, $\overline{|\nabla T|}_{\ell}\left(\vec{x}\right)$ is derivable n times but not $n+1$ (Arneodo et al., 1995). Consequently, we propose the use of singularity exponents as a proxy measure for the intensity of fronts, on the basis that the strongest fronts are those with the most marked singularity, hence, also those with the smallest singularity exponents.

The domain of the turbulent flow can be, then, divided into subsets according to their singularity exponent. This gives rise to the singularity spectrum, a concave function of h defined as

$$D\left(h'\right) \equiv d_F\left(\left\{\vec{x} | h\left(\vec{x}\right) = h'\right\}\right), \tag{3}$$

where $d_F(A)$ is the fractal dimension of set A. It follows that, the singularity spectrum $D(h)$ characterizes the "volume" occupied by fronts with intensity h. Moreover, the singularity spectrum $D(h)$ provides information about the statistical properties of SST. Indeed, the scaling properties of the moments of SST gradients are defined by a continuous function $\tau(p)$ of the moment order p

$$\langle \overline{|\nabla T|}_{\ell}^{p} \rangle \sim \left(\frac{\ell}{\ell_0}\right)^{\tau(p)}, \tag{4}$$

which is related to the singularity spectrum by a Legendre transform pair

$$\tau(p) = ph + d - D(h), \qquad \text{with} \qquad p = \frac{dD}{dh} \tag{5}$$

and

$$D(h) = ph + d - \tau(p), \qquad \text{with} \qquad h = \frac{d\tau}{dp}, \tag{6}$$

as shown by Parisi and Frisch (1985). It is worth mentioning that Equation 4 implies that the Probability Density Functions (PDF) of thermal gradients are dependent on the analysis scale ℓ, which is a signature of intermittency

(Frisch, 1995). As a consequence, care must be taken when analyzing PDF and kurtosis and when comparing PDF from data with different resolutions.

The singularity spectrum can also be related to the scaling of the structure functions of temperature, which are defined as

$$S_p(\ell) \equiv \langle |T_s\left(\vec{x}+\vec{\ell}\right) - T_s(\vec{x})|^p \rangle \tag{7}$$

and scale according to the continuous function $\zeta(p)$, that is,

$$S_p(\ell) \sim \left(\frac{\ell}{\ell_0}\right)^{\zeta(p)}. \tag{8}$$

using that, at small scales, $|T_s\left(\vec{x}+\vec{\ell}\right) - T_s\left(\vec{x}\right)| \sim \ell|\nabla T|$ it follows that,

$$\frac{1}{\ell_0^p}\langle |T_s\left(\vec{x}+\vec{\ell}\right) - T_s\left(\vec{x}\right)|^p \rangle \sim \left(\frac{\ell}{\ell_0}\right)^p \langle \overline{|\nabla T|}_\ell^p \rangle \sim \left(\frac{\ell}{\ell_0}\right)^p \left(\frac{\ell}{\ell_0}\right)^{\tau(p)} \sim \frac{1}{\ell_0^p}\left(\frac{\ell}{\ell_0}\right)^{\zeta(p)}, \tag{9}$$

with ℓ_0 being a constant, and consequently, both scaling functions are related by

$$\zeta(p) = p + \tau(p). \tag{10}$$

Recall that, the scaling of the structure function of order $p = 2$ gives the spectral slope of SST,

$$E(k) \propto k^{-\zeta(2)-1} = k^{-\tau(2)-3}, \tag{11}$$

where $E(k)$ is the energy spectrum and k the wavenumber (Frisch, 1995).

Guided by the recent work of Isern-Fontanet and Turiel (2021), here, we focus on two properties of the singularity spectrum: the most singular exponent h_∞,

$$h_\infty \equiv \min(h), \tag{12}$$

which is a measure of the intensity of the strongest fronts; and the width of the singularity spectrum defined as

$$\Delta h^- \equiv h_d - h_\infty, \tag{13}$$

where h_d is the mode. This quantity corresponds to the difference of slopes of $\zeta(p)$ between the origin ($p = 0$) and large orders ($p \to \infty$). Indeed, using Equation (6) and Equation (10), it can be seen that

$$\left.\frac{d\zeta}{dp}\right|_{p=0} - \left.\frac{d\zeta}{dp}\right|_{p\to\infty} = \left.\frac{d\tau}{dp}\right|_{p=0} - \left.\frac{d\tau}{dp}\right|_{p\to\infty} = h_d - h_\infty = \Delta h^-. \tag{14}$$

Therefore, the anomalous scaling, that is, the departure from a straight line increases with growing Δh^-.

3. Data and Procedures

SST fields were taken from numerical simulations of the circulation in the California Current System (see Figure 1a) generated with the ROMS oceanic model (Shchepetkin & McWilliams, 2005). The model was configured with a horizontal resolution of ~2.5 km (1,025 × 625 grid points) and 32 vertical levels with higher resolution in the upper layers. The boundary and initial conditions, as well as the forcing at the air-sea interface (wind stress and heat and freshwater fluxes) were derived from climatologies as in Capet et al. (2008). Singularity analysis was applied to snapshots of SST taken every two days of simulation spanning a period of two years.

Although very appealing, Equation (2) cannot be used directly to compute singularity exponents due to long-range correlations and discretization effects (Turiel et al., 2008). To avoid these difficulties, we used the method proposed by Pont et al. (2013) to compute singularity exponents (see Figure 1b). Then, the singularity spectrum of each snapshot of SST was computed within the domain of analysis (see red rectangle in Figure 1b) using the histogram method

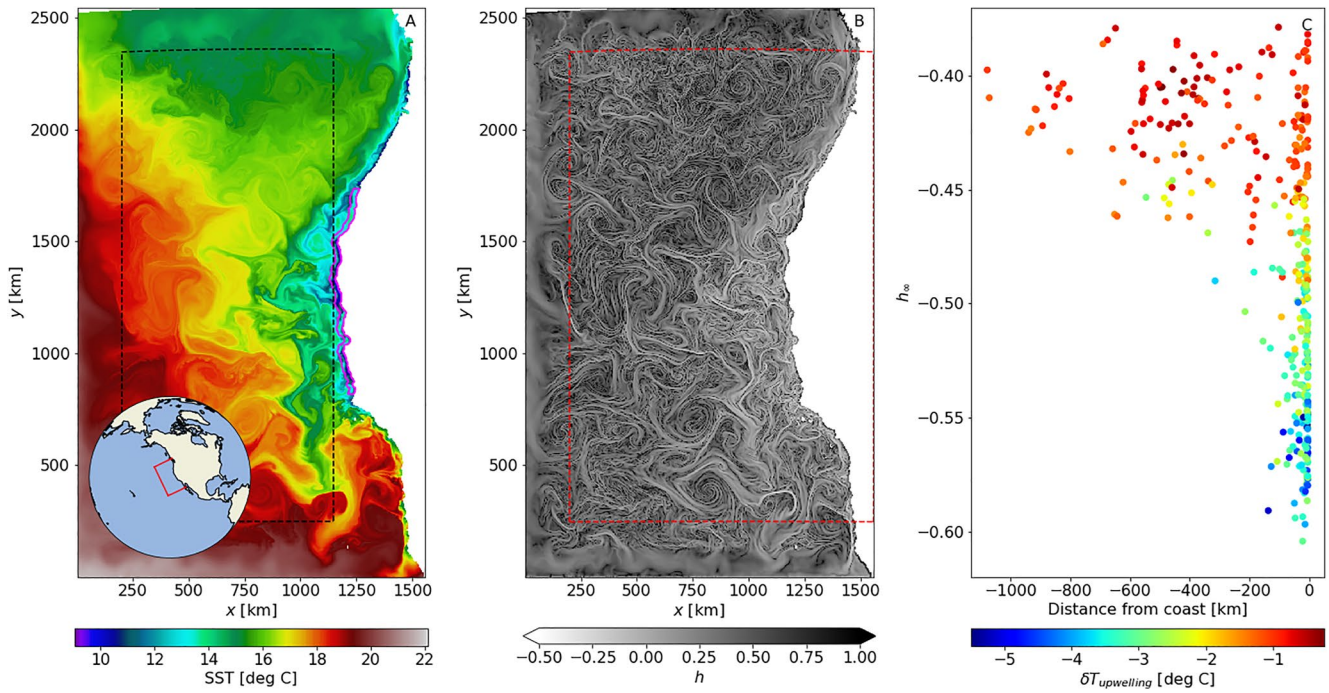

Figure 1. (a) Example of instantaneous Sea Surface Temperature (SST) corresponding to July 10th of the first year analyzed ($t = 20$ days) with the area used to compute Fourier spectra (black, dashed) and $\delta T_{upwelling}$ (purple, solid). The inset globe shows the geographical limits of the numerical simulations. (b) singularity exponents for the SST image with the area used to compute singularity spectra (red, dashed). The areas with blurred fronts in the open limits of the model are due to the low-resolution information imposed at the model open boundary conditions. (c) distance from coast of the h_∞ observed for the whole analyzed period with the color corresponding to $\delta T_{upwelling}$.

$$D(h_i) \approx d - \frac{\log N_i - \log N_{\max}}{\log(\ell/\ell_0)}, \tag{15}$$

where N_i is the number of grid cells having a singularity exponent in the range $[h_i - \frac{\delta h}{2}, h_i + \frac{\delta h}{2})$, $N_{\max}$ the number of valid ocean grid cells in the analysis domain, and $\ell/\ell_0 = \left(\sum_i N_i\right)^{\frac{1}{d}}$ (Turiel et al., 2006). The grid points surrounding the land mask were removed to avoid spurious values due to the land-sea transition and we used $d = 2$ and $\delta h = 0.02$ in the range from $h = -1$ to $h = 3$ for computing $D(h)$. Translational invariance was imposed to each singularity spectrum to correct for any shift that may exist in the singularity exponents (Isern-Fontanet & Turiel, 2021). This invariant condition consists in imposing that the $\langle|\overline{\nabla T}|_\ell\rangle$ does not depend on ℓ, that is, $\tau(1) \equiv 0$. Finally, the mode h_d was estimated by locally adjusting a parabola around the maximum of $D(h)$ and then, analytically calculating its maximum.

The function $\zeta(p)$ was derived from the instantaneous $D(h)$ by first applying the Legendre transform Equations (5) and, then, Equation (10). To reduce the spurious oscillations due to noise, we used a similar approach to the computation of h_d, that is, the Legendre transform was obtained by locally fitting a second order polynomial to the surroundings of each value of $D(h_i)$ and, then, analytically inverting it. On the contrary, the SST spectrum was computed independently from $D(h)$ using SST anomalies in the black box shown in Figure 1a, that is,

$$\delta T\left(\vec{x},t\right) = T\left(\vec{x},t\right) - \tilde{T}\left(\vec{x},t\right), \tag{16}$$

where $\tilde{T}\left(\vec{x},t\right) \equiv a_x(t)x + a_y(t)y + a_{xy}(t)xy + a_0(t)$ was estimated by least-squares fitting to SST in the whole domain. This form for $\tilde{T}\left(\vec{x},t\right)$ was selected due to the rotation of the grid to respect the geographical North. With the aim of having a simple measure of the intensity of the coastal upwelling, the temperature anomaly associated with it was defined as the mean temperature anomaly close to the coast, that is,

$$\delta T_{upwelling}(t) \equiv \langle \delta T\left(\vec{x},t\right)\rangle_{upwelling}. \tag{17}$$

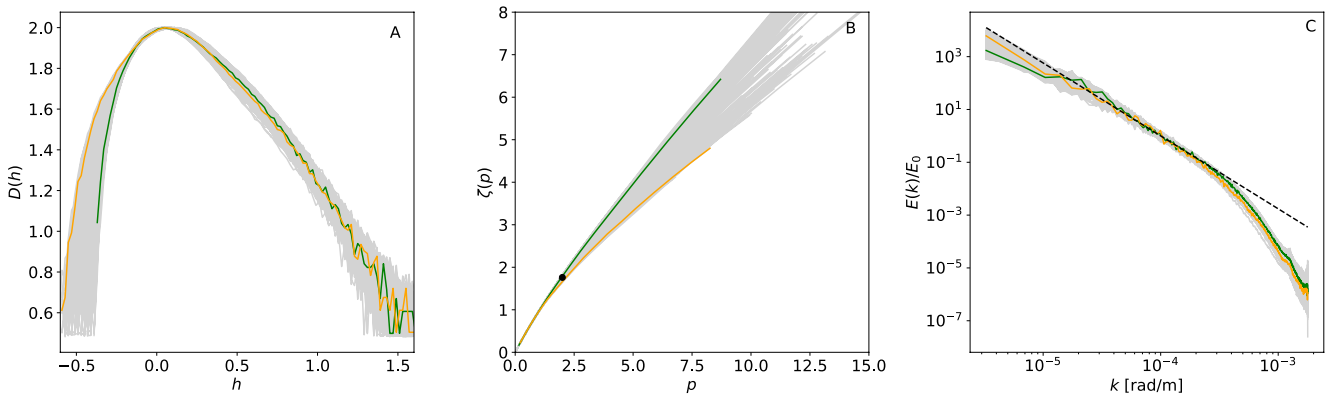

Figure 2. (a) Singularity spectra $D(h)$. (b) scaling of the structure functions of temperature $\zeta(p)$ derived from the singularity spectra. The black dot corresponds to $\langle\zeta(2)\rangle$. (c) normalized Fourier spectra. The black dashed line has a slope given by $-\langle\zeta(2)\rangle - 1$. Energy spectra are normalized by $E_0 \equiv E(k_0)$, where $k = 10^{-4}$ rad/m. Gray lines correspond to the observations for the full period, while orange and green lines correspond to the examples of two particular days: March 4th (green, $t = 246$ days) and August 23rd (orange, $t = 418$ days) of the second year.

This area was taken as the area between the coast and 10 grid points seawards (~25 km) and between $y = 810$ km and $y = 1{,}720$ km, which corresponds to the purple area marked in Figure 1a.

4. Results

Figure 1b unveils the complex structure of thermal fronts observable in a snapshot of SST, with the most intense fronts, bright lines in the figure, being those with smaller singularity exponents. The intensity of fronts has some spatial variability. On one side, the areas with blurred fronts found in the North, West, and South limits of the domain are due to the low-resolution information imposed at the model open boundary conditions. On the other, the intensity of fronts tend to be higher within the area strongly influenced by coastal upwelling (the area within [600 km, 1,150 km] × [700 km, 1,700 km] approximately). Moreover, results shown in Figure 1c reveal that the smallest values of h_∞ are concentrated close to the coast and correspond to large values of $|\delta T_{upwelling}|$, while larger values of h_∞ can be found away from the coast for and correspond to small values of $|\delta T_{upwelling}|$.

Singularity spectra $D(h)$ are asymmetric functions of h, whose properties change over time as revealed by Figure 2a. Indeed, the value of h_∞ ranges between −0.6 and −0.35 for the two years of simulation and the width Δh^- between 0.4 and 0.7. The changes in the width of $D(h)$ are related to changes in the anomalous scaling of the structure functions (Figure 2b) as expected from Equation 14. Such changes are more pronounced for moments larger than $p = 2$ (which provide the spectral slope of SST; Equation 11). Moreover, the slope of the instantaneous spectra of SST for $k < 10^{-4}$ rad/m, which has been computed independently, is close to the value given by the average $\langle\zeta(2)\rangle$ computed from the singularity spectra $D(h)$ (Figure 2c). The observed spectral slope is somewhat steeper than k^{-2}, in contrast to Capet et al. (2008). A shallower spectral slope can be recovered by reducing the spectral analysis to the area dominated by the upwelling, where fronts are stronger and more energy is present at the smaller resolved scales (not shown).

The two properties analyzed in this study, h_∞ and Δh^- are not independent but are strongly correlated with a linear correlation of −0.98 and a slope between them of −1.13 (Figure 3a). A closer look, however, shows that the snapshots with $h_\infty < -0.5$ have weaker slopes between h_∞ and Δh^- (−1.11) and a tendency to have larger values of $|\delta T_{upwelling}|$ (3.56 deg C on average) than snapshots with $h_\infty > -0.5$ (−1.14 and 1.66 deg C on average, respectively). Besides, the temporal evolution of h_∞ follows a seasonal cycle (Figure 3b), which has associated with a seasonal variation of the width of the singularity spectrum of SST gradients and thus, a seasonal variation of the anomalous scaling of the structure functions of temperature. Moreover, the close relation between the spatial location of h_∞ and $\delta T_{upwelling}$ shown in Figure 1c suggests a strong relationship between them, which is confirmed statistically: the Pearson correlation coefficient between the temporal evolution of h_∞ and $\delta T_{upwelling}$ (Figure 3b) is 0.87.

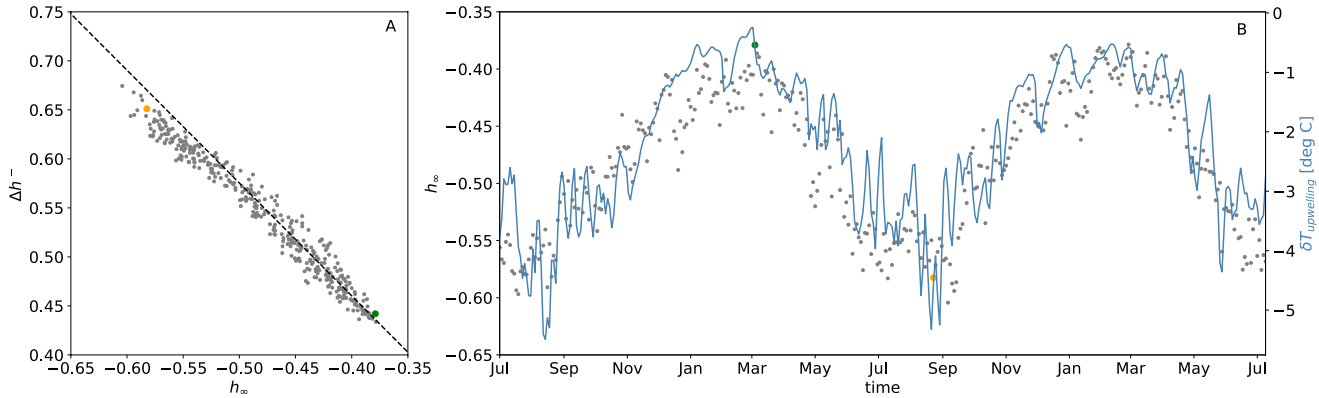

Figure 3. (a) Scatter plot between h_∞ and Δh^-. The black line corresponds to a slope of -1.13. (b) temporal evolution of h_∞ and $\delta T_{upwelling}$. Gray points correspond to the observations for the full period, while orange and green points correspond to the examples of two particular days: March 4th (green, $t = 246$ days) and August 23rd (orange, $t = 418$ days) of the second year.

5. Discussion

In this study, we have proposed, for the first time, to measure the intensity of fronts in SST using the singularity exponents of thermal gradients. Singularity exponents characterize the scaling at small scales, are independent of the gradient magnitude, and measure the degree of continuity of the field. Moreover, singularity exponents have the advantage over other popular approaches for detecting fronts, such as those based on histograms or gradient filters like the Sobel filter (Chang & Cornillon, 2015; Kirches et al., 2016), that they can be easily connected to statistical quantities that are central to turbulence theories (Section 2). Indeed, the singularity spectrum, which gives the fractal dimension of those points with the same exponent, emerges as a fundamental property of the ocean providing the link between anomalous scaling and the intensity of fronts. Here, we have exploited this relationship to understand the seasonal variability of the scaling of the structure functions in the California Current System.

Two main results have been reported in this study. First, there is a seasonal variability in the value of the most singular (the smallest) singularity exponent h_∞, which is well correlated with the evolution of the temperature anomaly associated with the upwelling $\delta T_{upwelling}$ (Figure 3b). Moreover, it has been observed that, for strong upwelling events, the strongest fronts are located close to the coast, while for weak upwelling events they can also be located offshore (Figure 1c), confirming then that the strongest fronts are generated by the upwelling process. The second main result is the existence of a linear correlation between the anomalous scaling of the structure functions measured by Δh^- and the most singular exponents h_∞ (Figure 3a). With the interpretation of singularity exponents as normalized measures of front intensity in mind (Section 2), our results imply that anomalous scaling are linearly anti-correlated to the intensity of the strongest fronts. Putting these two results together, it implies that some statistical properties of the flow in the area under study, including the spectral slopes of SST, are correlated to the intensity of the upwelling.

The seasonal variability of the upwelling front has been documented in previous studies (e.g., García-Reyes & Largier, 2012; Weber et al., 2021), so it could be foreseen that it was responsible for the seasonal variability of h_∞. Nevertheless, the present research unveils additional results that emphasize the importance of upwellings in setting up some of the statistical properties of the flow. This is due to the connection between front intensity and the anomalous scaling. Such a connection implies that those models unable to resolve the upwelling system would require some kind of parametrization to restore the variability of h_∞, as with other unresolved processes (e.g., Fox-Kemper et al., 2019). Still, the connection between h_∞ and Δh^- has more general implications since it gives also some clues on how to adjust ocean models. Indeed, according to the results presented here, the modification of eddy viscosity and eddy diffusivity not only would act on the intensity of fronts (e.g., Bodner et al., 2020) but also on the scaling properties of the structure functions (Figure 3a). Alternatively, those models with wrong front intensities will show wrong scaling properties of the structure functions. Besides, the scale independence of the framework used in the present study and the robustness of the algorithms for computing singularity exponents

(Pont et al., 2013) point to the use of the proposed approach to compare data and models with different resolutions and provide additional tools to investigate the dynamics of ocean fronts (McWilliams, 2021).

An important question that emerges is whether the correlation and slope between h_∞ and Δh^- is universal. A preliminary answer would be positive for two main reasons: the same correlation between h_∞ and Δh^- has been found for different variables, SST and velocities; and it has been found in regions with different dynamical regimes, the California Current System and the Gulf stream (see Isern-Fontanet & Turiel, 2021). To confirm this answer it would be necessary to analyze global numerical simulations (Su et al., 2020) or observations (Merchant et al., 2019). However, before using infrared SST measurements, it is necessary to address the problems generated by data gaps due to cloud coverage (Isern-Fontanet et al., 2021); the masking out of strong fronts by the failure of cloud mask algorithms (Kilpatrick et al., 2019); and the changes in Δh^- induced by noise (Isern-Fontanet & Hascoët, 2014). Among them, the most critical problem is the masking of strong fronts because it has a direct impact on the estimation of h_∞ and thus, $\Delta h^- = h_d - h_\infty$. Alternatively, the scale independence of these quantities opens the door to use microwave SST instead of infrared SST to assess the global validity of the results presented here.

6. Conclusions

Singularity exponents provide a measure of the intensity of SST fronts that can be connected to the scaling of the structure function and the spectral slope of SST through the singularity spectrum. When analyzing the numerical simulations of the California Current System, results show that the intensity of the most singular fronts is correlated to the anomalous scaling of the structure functions. These fronts, at their turn, are closely related to the seasonal change of intensity of the coastal upwelling characteristic of this area. Our study points to the need to correctly reproduce the intensity of the strongest fronts and, consequently, properly model processes such as coastal upwelling in order to reproduce correctly SST statistics in ocean models.

Data Availability Statement

The details of the model configuration, as well as, the simulated Sea Surface Temperatures generated for this study, and the singularity analysis described in Section 3 are available in https://doi.org/10.20350/digitalCSIC/14487 (Isern-Fontanet et al., 2022).

Acknowledgments
This work was supported by the Ministry of Economy and Competitiveness, Spain, and FEDER EU through the EXPLORA Ciencia National R + D Plan under TURBOMIX project (CGL2015-73100-EXP) and through the projects PROMISES (ESP2015-67549-C3-1-R) and COSMO (CTM2016-79474-R). This work was supported in part by the Spanish R&D project L-BAND (ESP2017-89463-C3-1-R), which is funded by MCIN/AEI/10.13039/501100011033 and ERDF. A way of making Europe, and project INTERACT (PID2020-114623RB-C31), which is funded by MCIN/AEI/10.13039/501100011033. We also acknowledge support from Fundación General CSIC (Programa ComFuturo). This work acknowledges the "Severo Ochoa Centre of Excellence" accreditation (CEX2019-000928-S). This work is a contribution to CSIC PTI Teledetect.

References

Arneodo, A., Bacry, E., & Muzy, J. F. (1995). The thermodynamics of fractals revisited with wavelets. *Physica A: Statistical Mechanics and its Applications*, *213*(1), 232–275. https://doi.org/10.1016/0378-4371(94)00163-N

Bodner, A. S., Fox-Kemper, B., Van Roekel, L. P., McWilliams, J. C., & Sullivan, P. P. (2020). A perturbation approach to understanding the effects of turbulence on frontogenesis. *Journal of Fluid Mechanics*, *883*, A25. https://doi.org/10.1017/jfm.2019.804

Callies, J., & Ferrari, R. (2013). Interpreting energy and tracer spectra of upper-ocean turbulence in the submesoscale range (1–200 km). *Journal of Physical Oceanography*, *43*(11), 2456–2474. https://doi.org/10.1175/JPO-D-13-063.1

Capet, X., McWilliams, J., Mokemaker, M., & Shchepetkin, A. (2008). Mesoscale to submesoscale transition in the California current system. Part I: Flow structure, eddy flux, and observational tests. *Journal of Physical Oceanography*, *38*, 29–43. https://doi.org/10.1175/2007jpo3671.1

Chang, Y., & Cornillon, P. (2015). A comparison of satellite-derived sea surface temperature fronts using two edge detection algorithms. *Deep Sea Research Part II: Topical Studies in Oceanography*, *119*, 40–47. https://doi.org/10.1016/j.dsr2.2013.12.001

Chenillat, F., Franks, P. J. S., Capet, X., Rivière, P., Grima, N., Blanke, B., & Combes, V. (2018). Eddy properties in the southern California current system. *Ocean Dynamics*, *68*(7), 761–777. https://doi.org/10.1007/s10236-018-1158-4

D'Asaro, E., Lee, C., Rainville, L., Harcourt, R., & Thomas, L. (2011). Enhanced turbulence and energy dissipation at ocean fronts. *Science*, *332*(6027), 318–322. https://doi.org/10.1126/science.1201515

Deser, C., Alexander, M., Xie, S., & Phillips, A. (2010). Sea surface temperature variability: Patterns and mechanisms. *Annual Review of Marine Science*, *2*, 115–143. https://doi.org/10.1146/annurev-marine-120408-151453

Fox-Kemper, B., Adcroft, A., Böning, C. W., Chassignet, E. P., Curchitser, E., Danabasoglu, G., et al. (2019). Challenges and prospects in ocean circulation models. *Frontiers in Marine Science*, *6*, 65. https://doi.org/10.3389/fmars.2019.00065

Frisch, U. (1995). *Turbulence: The legacy of A.N. Kolmogorov*. Cambridge University Press.

García-Reyes, M., & Largier, J. L. (2012). Seasonality of coastal upwelling off central and northern California: New insights, including temporal and spatial variability. *Journal of Geophysical Research*, *117*(C3). https://doi.org/10.1029/2011JC007629

Gulev, S., Thorne, P., Ahn, J., Dentener, F., Domingues, C., Gerland, S., et al. (2021). Climate change 2021: The physical science basis contribution of working group i to the sixth assessment report of the intergovernmental panel on climate change. In V. MassonDelmotte, et al. (Eds.). *Chap. Changing state of the climate system*. Cambridge University Press.

Isern-Fontanet, J., Ballabrera-Poy, J., Turiel, A., & García-Ladona, E. (2017). Remote sensing of ocean surface currents: A review of what is being observed and what is being assimilated. *Nonlinear Processes in Geophysics*, *24*, 613–643. https://doi.org/10.5194/npg-24-613-2017

Isern-Fontanet, J., Capet, X., Turiel, A., Olmedo, E., & González-Haro, C. (2022). Simulated sea surface temperature and derived singularity exponents for the California current system (v.1.0) [dataset]. https://doi.org/10.20350/digitalCSIC/14487

Isern-Fontanet, J., García-Ladona, E., González-Haro, C., Turiel, A., Rosell-Fiechi, M., Company, J., & Padial, A. (2021). High resolution ocean currents from sea surface temperature observations: The Catalan sea (Western mediterranean). *Remote Sensing*, *13*, 3635. https://doi.org/10.3390/rs13183635

Isern-Fontanet, J., & Hascoët, E. (2014). Diagnosis of high resolution upper ocean dynamics from noisy sea surface temperature. *Journal of Geophysical Research:Oceans*, *118*, 1–12. https://doi.org/10.1002/2013JC009176

Isern-Fontanet, J., Shinde, M., & González-Haro, C. (2014). On the transfer function between surface fields and the geostrophic stream function in the mediterranean sea. *Journal of Physical Oceanography*, *44*, 1406–1423. https://doi.org/10.1175/JPO-D-13-0186.1

Isern-Fontanet, J., & Turiel, A. (2021). On the connection between intermittency and dissipation in ocean turbulence: A multifractal approach. *Journal of Physical Oceanography*, *51*(8), 2639–2653. https://doi.org/10.1175/JPO-D-20-0256.1

Isern-Fontanet, J., Turiel, A., García-Ladona. & Font, J. (2007). Microcanonical multifractal formalism: Application to the estimation of ocean surface velocities. *Journal of Geophysical Research*, *112*, C05024. https://doi.org/10.1029/2006JC003878

Ivanov, L. M., Collins, C. A., Marchesiello, P., & Margolina, T. M. (2009). On model validation for meso/submesoscale currents: Metrics and application to roms off central California. *Ocean Modelling*, *28*(4), 209–225. https://doi.org/10.1016/j.ocemod.2009.02.003

Kilpatrick, K. A., Podestá, G., Williams, E., Walsh, S., & Minnett, P. J. (2019). Alternating decision trees for cloud masking in modis and viirs nasa sea surface temperature products. *Journal of Atmospheric and Oceanic Technology*, *36*(3), 387–407. https://doi.org/10.1175/jtech-d-18-0103.1

Kirches, G., Paperin, M., Klein, H., Brockmann, C., & Stelzer, K. (2016). Gradhist —A method for detection and analysis of oceanic fronts from remote sensing data. *Remote Sensing of Environment*, *181*, 264–280. https://doi.org/10.1016/j.rse.2016.04.009

Mahadevan, A. (2016). The impact of submesoscale physics on primary productivity of plankton. *Annual Review of Marine Science*, *8*(1), 161–184. PMID: 26394203. https://doi.org/10.1146/annurev-marine-010814-015912

McWilliams, J. C. (2021). Oceanic frontogenesis. *Annual Review of Marine Science*, *13*(1), 227–253. PMID: 33395349. https://doi.org/10.1146/annurev-marine-032320-120725

Merchant, C. J., Embury, O., Bulgin, C. E., Block, T., Corlett, G. K., Fiedler, E., et al. (2019). Satellite-based time-series of sea-surface temperature since 1981 for climate applications. *Scientific Data*, *6*(1), 223. https://doi.org/10.1038/s41597-019-0236-x

Parisi, G., & Frisch, U. (1985). On the singularity structure of fully developed turbulence. In M. Ghil, R. Benzi & G. Parisi (Eds.), *Turbulence and predictability in geophysical fluid dynamics. proc. intl. school of physics e. fermi* (pp. 84–87). North Holland.

Pont, O., Turiel, A., & Yahia, H. (2013). Singularity analysis of digital signals through the evaluation of their unpredictable point manifold. *International Journal of Computer Mathematics*, *90*(8), 1693–1707. https://doi.org/10.1080/00207160.2012.748895

Pope, S. B. (2000). *Turbulent flows*. Cambridge University Press. https://doi.org/10.1017/CBO9780511840531

Shchepetkin, A., & McWilliams, J. (2005). The regional oceanic modeling system (roms): A split-explicit, free-surface, topography-following-coordinate oceanic model. *Ocean Modelling*, *9*(4), 347–404. https://doi.org/10.1016/j.ocemod.2004.08.002

Skákala, J., Cazenave, P. W., Smyth, T. J., & Torres, R. (2016). Using multifractals to evaluate oceanographic model skill. *Journal of Geophysical Research: Oceans*, *121*(8), 5487–5500. https://doi.org/10.1002/2016JC011741

Skákala, J., Smyth, T. J., Torres, R., Buckingham, C. E., Brearley, A., Hyder, P., & Coward, A. C. (2019). Sst dynamics at different scales: Evaluating the oceanographic model resolution skill to represent sst processes in the southern ocean. *Journal of Geophysical Research: Oceans*, *124*(4), 2546–2570. https://doi.org/10.1029/2018JC014791

Su, Z., Torres, H., Klein, P., Thompson, A. F., Siegelman, L., Wang, J., et al. (2020). High-frequency submesoscale motions enhance the upward vertical heat transport in the global ocean. *Journal of Geophysical Research: Oceans*, *125*(9), e2020JC016544. https://doi.org/10.1029/2020JC016544

Sukhatme, J., Chaudhuri, D., MacKinnon, J., Shivaprasad, S., & Sengupta, D. (2020). Near-Surface ocean kinetic energy spectra and small-scale intermittency from ship-based ADCP data in the Bay of Bengal. *Journal of Physical Oceanography*, *50*(7), 2037–2052. https://doi.org/10.1175/JPO-D-20-0065.1

Turiel, A., Pérez-Vicente, C. J., & Grazzini, J. (2006). Numerical methods for the estimation of multifractal singularity spectra on sampled data: A comparative study. *Journal of Computational Physics*, *216*(1), 362–390. https://doi.org/10.1016/j.jcp.2005.12.004

Turiel, A., Yahia, H., & Pérez-Vicente, C. J. (2008). Microcanonical multifractal formalism—A geometrical approach to multifractal systems: Part I. Singularity analysis. *Journal of Physics A: Mathematical and Theoretical*, *41*(1), 015501. https://doi.org/10.1088/1751-8113/41/1/015501

Weber, E. D., Auth, T. D., Baumann-Pickering, S., Baumgartner, T. R., Bjorkstedt, E. P., Bograd, S. J., et al. (2021). State of the California current 2019–2020: Back to the future with marine heatwaves? *Frontiers in Marine Science*, *8*. https://doi.org/10.3389/fmars.2021.709454

Yu, K., Dong, C., & King, G. P. (2017). Turbulent kinetic energy of the ocean winds over the kuroshio extension from quikscat winds (1999–2009). *Journal of Geophysical Research: Oceans*, *122*(6), 4482–4499. https://doi.org/10.1002/2016JC012404